Use of steady-state setup for assessing the internal optical properties of non-spherical apple samples.

Mohamed Lamine Askoura[a,b*], Fabrice Vaudelle[b**], Jean-Pierre L'Huillier[b]

[a] Univ Bretagne Loire, Unité de Recherche GRAPPE, Ecole Supérieure d'Agricultures (ESA)-INRA, 55 rue Rabelais, BP 30748, 49007 Angers Cedex, France.

[b] Univ Bretagne Loire, Ecole Nationale Supérieure des Arts et Métiers (ENSAM.), Laboratoire Arts et Métiers ParisTech Angers (LAMPA.), 2 Boulevard du Ronceray, BP 93525, 49035 Angers cedex 01, France.

*ml.askoura@gmail.com , ** f.vaudelle@libertysurf.fr

Abstract: The aim of this paper is to retrieve the absorption (μ_a) and reduced scattering (μ'_s) coefficients of whole apples which exhibit a complex shape. To this end, the effect of the local boundary curvature is analyzed with Monte Carlo simulations and by measurements on apple species. A first attempt was made by performing simulations through an apple-like spheroid model covered with a thin skin layer of thickness 80 µm. Monte Carlo data were then analyzed to depict the changes of photon densities, diffusively reflected images and optical properties as a function of the light source location over the surface of such target. Second, spatially-resolved backscattered images were acquired from 207 "Royal Gala", and the values of μ_a and μ'_s were retrieved using an inverse algorithm to fit the scattering profiles with a diffusion theory model at the wavelength of 633 nm, in a selected fitting range of 2.8–10 mm. The results confirm the theoretical prediction and show that the absorption coefficient μ_a may be overestimated, while the reduced scattering coefficient μ'_s is slowly changed when the measurements are performed on these apples species. Finally, experiments carried out on 200 apples still show that μ'_s is negatively correlated to the fruit firmness with a correlation coefficient (r) of 0.63. The spatially-resolved technique provides an efficient means for measuring the optical properties of fruits, and may be also useful for assessing the apple firmness.

Keywords: Imaging system; light propagation; optical properties; diffusion theory; apple firmness.

doi:10.1016/j.compag.2018.12.049

1. Introduction

Optical techniques previously devoted to assess the optical properties of biological tissues (Cheong *et al.,* 1990; Tuchin *et al.,* 1997; Jacques, 2013), have been widely adapted and used to explore the quality of food and agricultural products (Nicolaï *et al.,* 2007). Since the first work reported by Norris (1964), the most agricultural applications of the near-Infrared (NIR) spectroscopy have been focused on the non-destructive measurements of several chemical constituents such as moisture, soluble solids, acid, and chlorophyll (Nicolaï *et al.,* 2007; Fu and Ying, 2014).

In the visible and near-Infrared wavelength window (600-1000nm), light propagation in biological tissues or fruits mainly depends on absorption and scattering processes. These complex events may be globally characterized by two macroscopic optical coefficients: the absorption (μ_a) and the reduced scattering (μ'_s) (Jacques, 2013; Mishchenko and Tuchin, 2009).

Absorption is related to some important chemical quality attributes (or chromophores) of the fruit, while scattering is usually caused by random microstructure properties and refractive index in tissue. The absorption coefficient of the fruits can vary strongly over the wavelength range of 400 to 1000 nm, whereas the reduced scattering coefficient decreases monotonically with wavelength (according to the Mie Theory).

For quality inspection of agricultural products it is essential to retrieve and uncouple (as much as possible) these two parameters. In this field, several works based on time-resolved reflectance spectroscopy (Cubeddu *et al.,* 2001(a); Cubeddu *et al.,* 2001(b); Valero *et al.,* 2004), spatially-resolved analysis (Qing *et al.*, 2008; Cen and Lu, 2009; Nguyen Do Trong *et al.,* 2014; Askoura *et al.,* 2015; 2016a), and integrating sphere technique combined with inverse adding-doubling method (Saeys *et al.,* 2008; Rowe et al., 2014), have been reported. While the inverse

adding-doubling method is considered as particularly interesting when the problem of the escaping light from the edge is resolved (Rowe et al., 2014), it is an invasive process contrary to the other methods cited above. Among these methods, the steady-state spatially resolved spectroscopy use the light intensities recorded at different surface locations to retrieve the optical properties of the interrogated samples.

Qin and Lu (2008) proposed a novel spatially-resolved hyperspectral diffuse imaging technique for measuring optical properties of many fruits (apple, peach, and pear) and vegetable samples. Lu and Peng (2006), Peng and Lu (2007a; 2007b; 2008), Mendoza *et al.,* (2011), Sun *et al.,* (2015), recorded and treated scattering images at multiple wavelengths in order to predict fruits (peach, apple) firmness and soluble solids content. Although the imaging set-up response has been well corrected by means of mathematical models (see Peng and Lu, 2007a; 2007b; 2008), the method used to retrieve the fruit optical properties still need to be improved. For example apples generally exhibit a convex shape which cannot be assimilated to a plane. However, spatially resolved imaging system are sensitive to the flatness of the sensing boundary, because absorption and scattering information are acquired from an inverse algorithm based on a semi-infinite diffusion model. During their growth up to the maturity phase, some faces of the fruits will not be exposed to solar radiations. This suggests that the optical properties to be recovered may be spatially-dependent. Moreover, distinctive skin pigment spots can also affect reflectance measurements and consequently influence the absorption and diffusion information related to the fruit. These different aspects must be taken into account when estimating the optical parameters of the apple flesh.

To describe the distinct features of the apples by means of their retrieved optical properties, some aspects related to the steady-state imaging setup on fruits need to be investigated. This includes to quantify the light reflectance and the level of light penetration inside the flesh tissue. Optical simulations based on the radiative transport of light in fruit tissue have been applied

only on semi-infinite (Baranyai and Zude, 2009; Qin and Lu, 2009) or spherical (Fraser et al., 2003; Vaudelle and L'Huillier, 2015; Ding et al., 2016) turbid media. Therefore, the specific objectives of this work are related to the assessment of the internal optical properties of apple samples having a complex boundary profile. First, a Monte Carlo code adapted to diffusing object with a shape like a spheroid was used to analyze synthetic scattering image. Second, apples were characterized by 3D experimental measurement of their optical properties. Finally, a relationship between optical properties and quality parameters was established.

2 Materials and methods

2.1 Monte Carlo model

A non-spherical apple geometry was modeled using two half-spheroids having the same axis with a common radius L/2 of 30mm, while the radii defined on the second normal axis are $L_1/2$=15mm and $L_2/2$=50mm (Fig. 1(a)). All that mimics a non-spherical apple covered with a thin skin layer of thickness 80µm. A ballistic light source of diameter 1mm irradiates the surface of this "apple", and the radiative transport of photons was performed with a Monte Carlo code. Each simulation launched 2.10^6 "photons" which propagate step by step until they either are absorbed or reach the interfaces flesh-skin and air-skin. The processes of scattering and absorption inside the tissue follow the rules needed by Monte-Carlo code propagation as the ones described in Ref Wang *et al.* (1995). For each layers, it is necessary to define the coefficients μ_a (absorption coefficient) and μ_s (scattering coefficient). They permit to build a step-size s and also the decreasing weight of "photon" linked to a "Russian roulette" test, which decides to follow the "photon" or to consider it as absorbed. Inside a homogeneous volume, a step-size s=-ln(ε)/(μ_a+μ_s) is computed from a random variable ε in the interval]0, 1]. The step-size s is modified when the photon path crosses an interface.

Some difficulties appear when a boundary differs from the one of a semi-infinite plane medium. The determination of the intersection point for which a "photon" hits spheroid surfaces and the computation of the direction change due to Fresnel reflection are carried out as described in the work of Vaudelle (2018). Nevertheless, the solution of the spheroid quadratic equation (finding the modified step-size s from the initial photon location up to the boundary) is performed here by an iterative procedure in order to prevent large errors of numerical computation that can occur when the step-size of propagation is very small with respect to the considered spheroid radii.

For the skin and flesh layers, the anisotropy coefficient $g=1-\mu'_s/\mu_s$ linked to the Henyey-Greenstein phase function $p(\alpha_p)=(1-g^2)/[4\pi(1+g^2-2g\cos\alpha_p)^{3/2}]$, where α_p is a polar angle, was set to 0.8, and the refractive index used to compute the angles of reflection from the interface air-skin was set to 1.4. The anisotropy coefficient g=0.8 used here is consistent with some experimental studies on apple tissues (Saeys et al., 2008; Askoura et al., 2016b) with g~0.7-0.8, and where the scattering coefficients μ_s are ~3 and ~15mm^{-1} for flesh and peel tissues, respectively. In fact, the retrieval of anisotropy coefficient can change according to the estimation of the scattering coefficient (Vaudelle, 2017). For instance, experimental values of g and μ_s cited in other studies (Van Beers et al., 2017; Vaudelle, 2018) are higher (g~0.9 and μ_s~12mm^{-1}) than those retained for the apple flesh tissue. Nevertheless, the chosen values of μ_s and g are not critical contrary to the one of $\mu'_s=\mu_s(1-g)$ because the source-detector distances of interest for usual devices are larger than $1/\mu'_s$. The skin layer (top layer) is characterized by the optical coefficients μ'_s=4mm^{-1}, μ_a=0.05mm^{-1}, whereas the flesh layer (bottom layer) is characterized by μ'_s=1mm^{-1} and μ_a=0.01mm^{-1}.

Photon densities inside the turbid medium and reflectance from the curved boundary were generated with the Monte Carlo code. The reflectance is recorded on a planar surface which is

tangent to the curved boundary on a point located at the center of the light source (Fig. 1a). Besides, the recording is processed upon a virtual pixel of size 0.1x0.1 mm². The reflectance intensity related to the scattering image corresponds to the local intensity multiplied by a local cosine projection. That mimics approximately the intensity detection performed by a camera, but also permits to get a light quantity theoretically proportional to the total light intensity related to a point of the curved surface. Five points of source location were chosen along the direction z, as shown in Fig. 1(b).

2.2 Experimental setup

The setup used to measure the optical parameters of the apple is illustrated in Fig. 2. It consists of a light source, a CCD camera and a goniometer system with two degrees of freedom (Fig. 2). The light beam of 1 mm diameter was generated by a He-Ne laser emitting at the wavelength of 633 nm with a beam power of 35 mW. The camera (Model C4880-21-24A, Hamamatsu Photonics Systems, Bridgewater, NJ, USA) was placed in the plane parallel to the laser beam, and used to capture the light scattered at each angular position (θ, ϕ). Apple initially undergoes a manual rotation angle ϕ (corresponding to φ+90°) varying between [30-150 °] with a step of 30°. At each rotation angle ϕ, the apple position was adjusted so that the laser beam remains always normal to the surface of the apple (Figs. 2a-2b). At each angle position ϕ, apple undergoes a second manual rotation angle θ, which was varied between [0 – 360°] with a step of 30°.

2.3 Diffusion model

Light propagation in biological materials is governed by the light transport equation (Tuchin, 2000). Interestingly, the diffusion approximation is valid for most fruits and vegetables because scattering is dominant over absorption ($\mu'_s >> \mu_a$). For a homogeneous semi-infinite turbid medium illuminated by an infinitely small continuous wave (CW) point light source, the diffuse

reflectance $R(\rho)$ at its surface depends on the source-detector distance ρ ($> 1/\mu'_s$) and the two optical parameters μ_a and μ'_s (Farrell *et al.*, 1992):

$$R(\rho) = \frac{1}{4\pi\mu_t'}\left[\left(\mu_{eff} + \frac{1}{r_1}\right)\frac{e^{-\mu_{eff} r_1}}{{r_1}^2} + \left(\frac{4}{3}A + 1\right)\left(\mu_{eff} + \frac{1}{r_2}\right)\frac{e^{-\mu_{eff} r_2}}{{r_2}^2}\right] \qquad (1)$$

where $\mu'_t = \mu'_s + \mu_a$ is the total optical transport coefficient, $\mu_{eff} = [3\mu_a\mu'_t]^{1/2}$ is the effective attenuation coefficient. The variables r_1 and r_2 are given by the following two equations, $r_1 = \sqrt{\left(\frac{1}{\mu_t'}\right)^2 + \rho^2}$, and $r_2 = \sqrt{\left(\frac{\frac{4}{3}A + 1}{\mu_t'}\right)^2 + \rho^2}$. The coefficient A has been introduced to take into account the internal reflection. Equation (1) is the theoretical basis used to fit the normalized profiles by means of a trust-region method. A nonlinear least squares curve fitting algorithm was implemented on Matlab.8.a to estimate the values of μ_a and μ'_s from the spatially-resolved reflectance profiles. In order to avoid the effects of both the skin and the beam size (Vaudelle *et al.*, 2017), but also of the detection threshold (~ two decades with a camera), a sensing range of distance ρ [2.8 – 10 mm] was selected to retrieve the optical coefficients (Askoura *et al.*, 2016c). Fig. 3 depicts an example of scattering image obtained from the Hamamatsu CCD camera using a spherical apple and the fit of the reflected intensity over the range of [2.8 – 10 mm]. In this sensing range, the relative fitting errors amount to 1-20% (depending on the optical properties) when a spherical object of typical diameter of 70mm is considered (Askoura *et al.*, 2016c).

2.4 Apple samples and analysis protocol of the firmness

2.4.1 Apple samples

The experiments were carried out on 207 Royal Gala cultivars. Seven apples were used to estimate the effect of the boundary curvature, while two hundreds ones were used to study the correlation between the optical properties measurements and firmness index. They are drawn

from a wider set in order to constitute a homogeneous group from the point of view of their coloring, masses, and sizes. The dark red color of apple was much more pronounced on the sunny side, while the seven samples exhibit approximately a conical shape (Fig. 2c).The average equatorial diameter was measured as 6.3 ± 19% cm, and height as 7.63 ± 13% cm. The apples were stored at 4 °C. Because the temperature of the fruit greatly influences their mechanical properties (Nadulski and Grochowicz, 1997), they were brought into the room 24 hours before the experiments in order to stabilize their temperature. Preliminary studies have shown that the thermal time constant is 4 to 10 hours.

2.4.2 Destructive Maturity/Quality Measurement

After image recording of fruits, firmness was measured by standard destructive methods at the same location where the scattering measurements had been carried out. Magness–Taylor (MT) fruit firmness (N) measurements were performed with a traction machine (MTS, Synergie 200H). Penetration speed was set at 50 mm min^{-1} and the test was stopped after penetration to 10 mm at a loading speed of 2 mm/s. The maximum displayed on the recorded force-deformation curve was used as a measure of fruit firmness.

2.4.3 Calibration models for firmness

Partial Least Squares (PLS) regression is a widely used chemometric method for building calibration models. PLS is suited well when the matrix of predictors has more variables than observations, and also when the input variables contain noise and are strongly correlated. PLS components are computed under the constraint of maximization of covariance between inputs and outputs. Therefore, it can provide a set of orthogonal factors that have the best predictive power from the combinations of different methods with an increased number of variables. Prior to the model development, samples were first sorted in ascending order for firmness. The sorted samples were then divided into two groups: 75% of the samples were used for calibration and the remaining 25% samples were used for independent validation (or prediction). In this study,

PLS models (i.e., selection of appropriate numbers of latent variables) were determined by full cross validation of the calibration set until the root-mean-square error of cross validation (RMSECV) reached minimum. All the processing were conducted in Matlab version 8.a (The Mathworks, Natick, USA).

3 Results and discussion

3.1 Effect of the boundary curvature

3.1.1 Monte Carlo model

The Figures 4(a-e) depict the photon densities and the scattering images related to 5 light source locations. The area around the position (a) and (b) correspond to the higher curvatures along the axis z than the other points, while the point (e) is linked to the higher curvature along the axis y. The lowest and highest average curvatures can be associated to the positions (d) and (a), respectively. It can be seen than the deeper light density and the larger area of reflectance occur when the curvature is small. For instance, an example of scattering image obtained with a commercial camera (very low resolution) illustrates the differences related to the opposite cases (d) and (a). Beside, a specific simulation (with μ_a=0.0113mm^{-1}, μ'_s=1.2mm^{-1} for the bottom layer and using 6.10^6 "photons") is performed to show that the modelling can reproduce the experimental case cited above for distances larger than $1/\mu'_s$ (Fig. 5).

Note that the real Cartesian coordinate system of the scattering images are (X, y). The profiles of all the 5 reflectance images are shown along the axis X and y in the Figs 6. (a) and (b), respectively. The curves are approximately merged for almost source positions in the case of the Fig. 6(a), contrary to the ones of the Fig. 6(b). So, the usual methods used to reduce a scattering image into a 1-D spatial scattering profile can be briefly restated: either by performing an integration along lines with low curvature and with a few parallel lines close to the source location (often at proximity ~1.5-1.6mm when saturation occurs) (Peng and Lu

2007), or by radial averaging computed from concentric circular band (Sun *et al.* 2015, Lu *et al.*, 2017).

The retrieval of optical coefficients, μ'_s and μ_a, with the help of the Farrell diffusion equation is performed using different integrating systems: about ten of integrating lines along X crossing the light source area, or at 1.6mm of the source area, and a radial averaging. The determination coefficient is always superior to 0.99 in the fitting process. The results are depicted in Fig. 7, and they show discrepancies for absorption coefficient. Whatever the integrating system, the retrieved values of μ_a increase when the sources are located over surface with high curvature, cases (a) and (b). It can be noted that the error is more important when the radial averaging is used. This last method was the one used to the fitting example in Fig. 3. The integrating lines along X is the one considered for the next section.

3.1.2 Experiments

Experimental and theoretical evolutions of μ_a and μ'_s are plotted against the angle ϕ (θ was kept constant) in Figs. 8 (a) and (b) respectively. It is shown that the absorption coefficient decreases and reaches a stable value from the angle ϕ =90°, and tends toward a value close to that retrieved on a plane. In contrast, the experimental reduced scattering coefficient barely increases from 1.10 to 1.13 mm^{-1}, while no increase is noticeable with the theoretical ones. These findings are also consistent with those reported by Vaudelle and L'Huillier, (2015), who performed Monte Carlo simulations on apples assimilated as a two layer spherical model including skin and flesh tissues.

Figs. 9(a) and (b) respectively show the evolution of retrieved absorption and reduced scattering coefficients plotted as a function of the angle θ, for five values of the angle ϕ equal to 30, 60, 90, 120, and 150 °. The data confirm that μ'_s is not sensitive along a section of the fruit studied. This seems to show that the fruit structure does not change circumferentially. On the contrary,

the absorption coefficient μ_a presents variations (depending on the angle θ) which may be attributed to different exposures of the fruit to the radiations emitted by the sun. It is well known that the absorption spectrum of apple cultivars above all presents two remarkable peaks over a wavelength range spanning 400-1000 nm (Nicolaï *et al.,* 2007). The former corresponds to Chlorophyll-a, and can be seen at 670 nm with absorption values ranging from 0.003 up to 0.039 mm^{-1}. The second is related to water absorption on apples which ranges from 0.025 mm^{-1} to 0.052 mm^{-1}. According to Merzlyak *et al.,* (2003), other absorption peaks located at 425 nm, 450 nm, and 480 nm correspond to combination of Chlorophyll-a and Carotenoids, with typical absorption values ranging from 0.09 mm^{-1} to 0.145 mm^{-1} at 450 nm. Then, lower absorption values are expected when apple samples are studied at 630 nm, as is the case of the Royal Gala for which the recovered μ_a ranges from 0.015 mm^{-1} to 0.007 mm^{-1}. Previous studies based on different optical techniques have reported similar apple tissue absorption (~0.1-0.0025 mm^{-1}) at the working wavelength of 630 nm (Qin and Lu 2008, Saeys *et al.,* 2008, Rowe *et al.,* 2014, Cubeddu *et al.,* 2001b). In the same way, the μ'_s value of about 1.12 mm^{-1} is also consistent with those reported by Rowe *et al.,* (2014), and Saeys *et al.,* (2008) for the Royal Gala.

3.2 Prediction of apple firmness using optical properties

Prediction results for the fruit firmness of Royal Gala using μ'_s are shown in Fig. 10 (around the smallest curvature area). This reveals a negative correlation between μ'_s and the maximum force Ft. The regression line shown in red color has an equation form: y = -0.04x + 2.75 (slope in mm^{-1}/N). The correlation between μ'_s and Ft is equal to -0.63 (the root-mean-square error and bias of prediction are 6 N and 0.5 N, respectively). This correlation is significant (p. value <0.01). This result is in agreement with the findings reported by Vanoli *et al.,* (2010), and Rowe *et al.,* (2014) who established correlations equal to -0.70, and -0.68, respectively. In contrast, Sun *et al.,* (2015) and (2016), used a camera and recording on concentric circular bands. They established correlations ranging from -0.15 to + 0.5 by considering the whole apple (Royal

Gala), and -0.57 to -0.64 for the case of the cut one. They suggested that the skin and the curved surface of the sample may contribute to distort their results.

It should be noted that the signals detected close to the illumination spot are dominated by photons which only have interacted with the superficial layers (skin, sub-surface) of the sample (Nguyen Do Trong *et al.,* 2014). Photons recorded at further distances from the illumination point will have probed deeper into the flesh and will contain more internal information in comparison to shorter distances (Ding *et al.*, 2016). However, if the source-detector distance is too large, the recorded signals are weakened (low SNR) but are also more influenced by the local curvature of the apple sample (Vaudelle and L'Huillier, 2015). As a result, an optimal sensing range is required. This important point for the Vis/NIR spectroscopy has been recently well documented by Van Beers *et al* (2015) in order to predict maturity-related quality parameters of Braeburn apple varieties. They also showed that for firmness, which is mainly related to the flesh, larger distance from the illumination spot allowed better correlations. We note that our findings have been obtained by using an optimal sensing range of axial distance 2.8-10 mm always around the smallest curvature area, which seems to be a good compromise to reduce the effect of both boundary curvature and skin layer of the studied apple sample.

4 Conclusions

These preliminary studies show that when the radius of curvature of the measurement area is small (~ <15 mm), there is an overestimation of the absorption coefficient μ_a, while the reduced scattering coefficient μ'_s is less influenced. These findings confirm the results obtained by the Monte Carlo method. It seems interesting to carry out measurements by seeking flattened areas on the fruit, and by making measurements at many areas over the surface of the fruit. In these conditions, statistical analyses also show a negative correlation between the μ'_s and the maximum force Ft recorded with the Magness–Taylor penetrometer device. The spatially resolved imaging method provides an efficient means for measuring the optical properties of

fruits, and seems also useful for assessing fruit quality attributes. However, using combination of different data at multiple wavelengths might be useful to improve the correlations between optical properties and fruit firmness.

Acknowledgements

This work was funded by the Regional Council of Pays de la Loire and supported by the AI fruit Project. The authors thank Rémy Aurand and Ronan Symoneaux for their help in the apple firmness investigation.

References and links

Askoura, M.L., Piron, V., Vaudelle, F., L'Huillier, J.-P., Madieta, E., Mehinagic, E. (2015). Experimental investigation on light propagation through apple tissue structures Proc. SPIE 9542, Medical Laser Applications and Laser-Tissue Interactions VII, pp. 954218-9542126.

Askoura, M.L., Vaudelle, F., L'Huillier, J.-P., (2016a). Experimental study of light propagation in apple tissues using a multispectral imaging system. Photonics 3, 50.

Askoura, M.L., Vaudelle, F., L'Huillier, J.-P., (2016b). Multispectral measurement of scattering angular light distribution in apple skin and flesh samples. Applied Optics 55 (32), 9217–9225.

Askoura, M.L., Vaudelle, F., L'Huillier, J.-P., (2016c). Numerical Study of Light Transport in Apple Models Based on Monte Carlo Simulations. Photonics 3, 2.

Baranyai L., Zude M., (2009). Analysis of laser light propagation in kiwifruit using backscattering imaging and Monte Carlo simulation. Computer and Electronics in Agriculture 69, 33-39.

Cen, H., Lu, R., (2009). Quantification of the optical properties of two-layer turbid materials using a hyperspectral imaging-based spatially-resolved technique. Applied Optics 48, 5612-5623.

Cheong, W. F., Prahl, S. A., & Welch, A. J. (1990). A review of the optical properties of biological tissues. IEEE Journal of Quantum Electronics, 26(12), 2166-2185.

Cubeddu, R., D'Andrea, C., Pifferi, A., Taroni, P., Torricelli, A., Valentini, G., & Valero, C. (2001a). Nondestructive quantification of chemical and physical properties of fruits by time-resolved reflectance spectroscopy in the wavelength range 650–1000 nm. Applied Optics, 40(4), 538-543.

Cubeddu, R., D'Andrea, C., Pifferi, A., Taroni, P., Torricelli, A., Valentini, G., & Johnson, D. (2001b). Time-resolved reflectance spectroscopy applied to the nondestructive monitoring of the internal optical properties in apples. Applied Spectroscopy, 55(10), 1368-1374.

Ding, C., Shi, S., Chen, J., Wei, W. and Tan, Z. (2016). Influence of surface curvature on light-based nondestructive measurement of stone fruit. Computer and Electronics in Agriculture, 121, 200–206.

Farrell, T.J., Patterson, M.S., Wilson, B., (1992). A diffusion theory model of spatially resolved, steady-state diffuse reflectance for the noninvasive determination of tissue optical properties in vivo. Medical Physics 19, 879-888.

Fraser, D. G., Jordan, R. B., Kunnemeyer, R., McGlone, V. A., (2003). Light distribution inside mandarin fruit during internal quality assessment by NIR spectroscopy. Postharvest Biology and Technology 27, 185-196.

Fu, X., Ying, Y., (2014). Food Safety Evaluation Based on Near Infrared Spectroscopy and Imaging: a Review, Critical Reviews in Food Science and Nutrition, DOI: 10.1080/10408398.2013.807418

Jacques, S. L. (2013). Optical properties of biological tissues: a review. Physics in Medicine and Biology, 58(11), R37.

Lu, R., Peng, Y., (2006). Hyperspectral scattering for assessing peach fruit firmness. Biosystems Engineering 93, 161-171.

Lu, Y., Huang, Y., and Lu, R., (2017). Innovative Hyperspectral Imaging-Based Techniques for Quality Evaluation of Fruits and Vegetables: A Review. Applied Science 7, 189; doi:10.3390.

Mendoza, F., Lu, R., Ariana, D., Cen, H., & Bailey, B. (2011). Integrated spectral and image analysis of hyperspectral scattering data for prediction of apple fruit firmness and soluble solids content. Postharvest Biology and Technology, 62(2), 149-160.

Merzlyak, M.N., Solovchenko, A.E., Gitelson, A.A. (2003). Reflectance spectral features and non-destructive estimation of chlorophyll, carotenoid and anthocyanin content in apple fruit. Postharvest Biology and Technology 27, 197-211.

Mishchenko, M.I., V. Tuchin., (2009). Tissue Optics: Light Scattering Methods and Instruments for Medical Diagnostics2nd ed2007SPIE PressBellingham, WAHardbound, ISBN 0-8194-6433-3, 841pp. Journal of Quantitative Spectroscopy and Radiative Transfer 110, 528.

Nadulski, R., Grochowicz, J., (1997). The impact of temperature on the mechanical properties of selected varieties of apples, III International Symposium on Sensors in Horticulture 562, pp. 209-212.

Nguyen Do Trong, N., Rizzolo, A., Herremans, E., Vanoli, M., Cortellino, G., 596 Erkinbaev, C., Tsuta, M., Spinelli, L., Contini, D., Torricelli, A., (2014). Optical properties–microstructure–texture relationships of dried apple slices: Spatially resolved diffuse reflectance spectroscopy as a novel technique for analysis and process control. Innovative Food Science & Emerging Technologies 21, 160-168.

Nicolai, B. M., Beullens, K., Bobelyn, E., Peirs, A., Saeys, W., Theron, K. I., Lammertyn, J. (2007). Nondestructive measurement of fruit and vegetable quality by means of NIR spectroscopy: A review. Postharvest Biology and Technology, 46(2), 99-118.

Norris, K. H. (1964). Design and development of a new moisture meter. Agric. Eng, 45(7), 370-372.

Peng, Y., & Lu, R. (2007a). Prediction of apple fruit firmness and soluble solids content using characteristics of multispectral scattering images. Journal of Food Engineering, 82(2), 142-152.

Peng, Y., Lu, R., (2007b). A recursive method for updating apple firmness prediction models based on spectral scattering images, Optics for Natural Resources, Agriculture, and Foods II, 67610U.

Peng, Y., Lu, R., (2008). "Analysis of spatially resolved hyperspectral scattering images for assessing apple fruit firmness and soluble solids content," Postharvest Biology and Technology, vol. 48, pp. 52-62.

Qin, J., Lu, R., (2008). Measurement of the optical properties of fruits and vegetables using spatially resolved hyperspectral diffuse reflectance imaging technique. Postharvest Biology and Technology 49, 355-365.

Qin, J., Lu, R., (2009). Monte Carlo simulation for quantification of light transport features in apples. Computers and Electronics in Agriculture 68, 44-51.

Qing, Z., Ji, B., Zude, M., 2008. Non-destructive analyses of apple quality parameters by means of laser-induced light backscattering imaging. Postharvest Biology and Technology 48, 215-222.

Rowe, P.I.; Künnemeyer, R.; McGlone, A.; Talele, S.; Martinsen, P.; Seelye, R, (2014). Relationship between tissue firmness and optical properties of “royal gala” apples from 400 to 1050 nm. Postharvest Biology and Technology., 94, 89–96.

Saeys, W., Velazco-Roa, M.A., Thennadil, S.N., Ramon, H., Nicolaï, B.M., (2008). Optical properties of apple skin and flesh in the wavelength range from 350 to 2200 nm, Applied Optics, pp. 908-919.

Sun, J., Künnemeyer, R., McGlone, A., Rowe, P., & Talele, S. (2015). Development of a multispectral imaging system for apple firmness prediction. In 2015 9th International Conference on Sensing Technology, IEEE doi: 10.1109/ICSensT.2015.7438390.

Sun, J., Künnemeyer, R., McGlone, A., Rowe, P. (2016). Multispectral scattering imaging and NIR interactance for apple firmness predictions. Postharvest Biology and Technology 119, 58-68.

Tuchin, V. V., Maksimova, I. L., Zimnyakov, D. A., Kon, I. L., Mavlyutov, A. H., & Mishin, A. A. (1997). Light propagation in tissues with controlled optical properties. Journal of Biomedical Optics, 2(4), 401-417.

Tuchin, V.V., (2000). Tissue optics : light scattering methods and instruments for medical diagnosis. SPIE Press, Bellingham, Wash.

Valero, C., Ruiz-Altisent, M., Cubeddu, R., Pifferi, A., Taroni, P., Torricelli, A., Valentini, G., Johnson, D., Dover, C., (2004). Selection models for the internal quality of fruit, based on time domain laser reflectance spectroscopy. Biosystems Engineering 88, 313-323.

Van Beers, R., Aernouts, B., Gutiérrez, L.L., Erkinbaev, C., Rutten, K., Schenk, A., Nicolaï, B., Saeys, W., (2015). Optimal illumination-detection distance and detector size for predicting Braeburn apple maturity from Vis/NIR laser reflectance measurements. Food and Bioprocess Technology 8, 2123-2136.

Van Beers, R., Aernouts, B., Watté, R., Schenk, A., Nicolai, B., Saeys, W., (2017). Effects of maturation on the bulk optical properties of apple skin and cortex in the 500-1850 nm wavelength range. J. Food Eng. 214, 79–89.

Vanoli, M., Rizzolo, A., Zerbini, P.E., Spinelli, L., Torricelli, A., (2010). Non-destructive detection of internal defects in apple fruit by time-resolved reflectancespectrscopy. Environmentally Friendly and Safe Technologies for Quality of Fruit and Vegetables, 20-26.

Vaudelle, F., L'Huillier, J.-P., (2015). Influence of the size and skin thickness of apple varieties on the retrieval of internal optical properties using VIS/NIR spectroscopy: A monte carlo-based study. Computer and Electronics in Agriculture, 116, 137–149.

Vaudelle, F. (2017). Approximate analytical effective phase function obtained for a thin slab geometry. J. Quant. Spectrosc. Radiat. Transfer 193, 47–56.

Vaudelle, F., L'Huillier, J.-P., Askoura, M.L., (2017). Light source distribution and scattering phase function influence light transport in diffuse multi-layered media. Optics Communications, 392, 268–281.

Vaudelle, F. (2018). Light scattering in thin turbid tissue including macroscopic porosities: A study based on a Monte Carlo model. Optics Communications, 425, 91–100.

Wang, L., Jacques, S.L., Zheng, L., (1995). MCML-Monte Carlo modeling of light transport in multi-layered tissues. Comput. Methods Prog. Biomed, 47, 131–146.

Figure Captions

Fig. 1. Schematic depictions of (a) the non-spherical object and the imaging system used in the Monte Carlo code, and (b) the set of light source locations. The lengths used are L_1=30mm, L_2=100mm and L=60mm.

Fig. 2. Illustration of the procedure used to measure apple optical parameters according to the local radius of curvature. (a) Photography of the setup. (b) Measurement example for different angles ϕ and θ. (c) Angular discretization of the chosen measurement points.

Fig. 3. Typical scattering image related to a spherical apple (a) and fitting curve (b) of experimental data using equation (1) to estimate the optical properties.

Fig. 4. Simulation results linked to the scheme described in Fig. 1. (a-e) In-depth photon densities and backscattered images corresponding to 5 light source locations. (f) Illustration of experimental observation obtained with an apple of complex shape (independent of those considered in the section 2.4) and with the help of a low resolution camera.

Fig. 5. Comparison of experimental cases shown in Fig. 4(f) with Monte Carlo simulations using μ_a=0.0113mm^{-1}, μ_s'=1.2mm^{-1} for the bottom layer and 6.10^6 launched "photons".

Fig. 6. Reflectance profile intensities related to the scattering images depicted in Fig. 4(a-e) along the axis X (a) or the axis y (b).

Fig. 7. Estimates of the optical coefficients from a spatial 1-D profile obtained by three integrating systems: (a) Example of scattering image, where integrating lines along the direction X are drawn; (b) absorption coefficient (up) and reduced scattering coefficient (down).

Fig. 8. Optical coefficients retrieved from the experimental procedure (as described in Fig. 2) versus the angle ϕ (θ=0°) and averaged data generated by means of Monte Carlo code (cases shown in Fig. 7 where integration lines along the direction X cross the positions (X=0,y=0) and (X=0,y= ±1.6mm)). (a) Evolution of the absorption coefficient μ_a. (b) Evolution of the reduced scattering coefficient μ'_s.

Fig. 9. Evolution of the optical coefficients plotted against the angles ϕ and θ: (a) absorption coefficient μ_a. (b) reduced scattering coefficient μ'_s .

Fig. 10. Plot of the firmness of 200 `Royal Gala' apples against the estimated reduced scattering coefficient μ'_s.

(a)

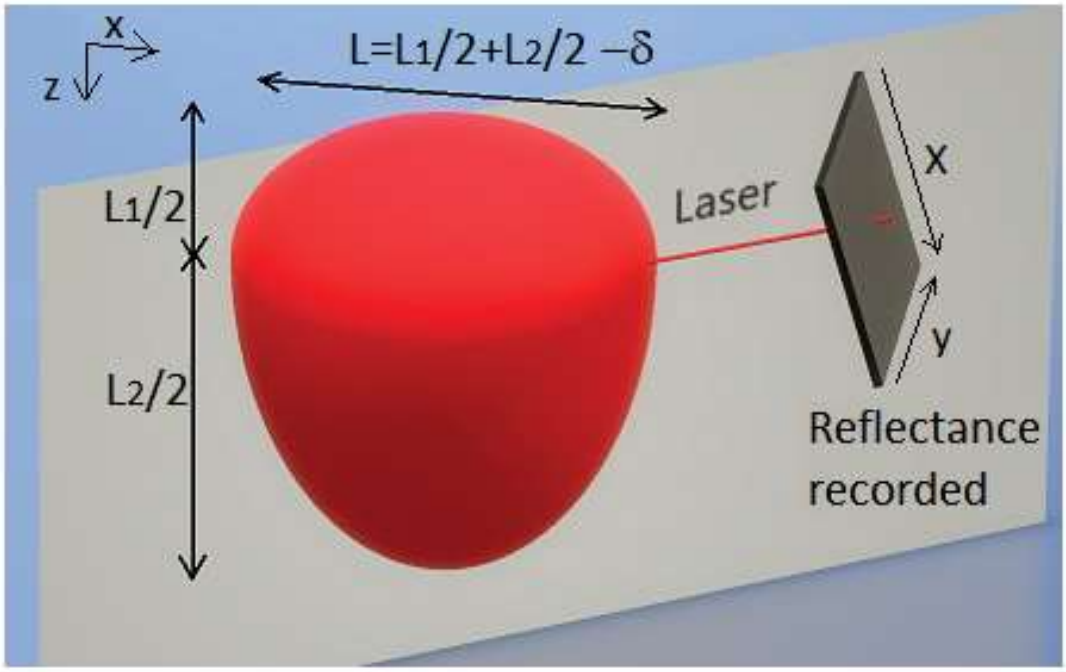
x
z
L=L1/2+L2/2 −δ
L1/2
L2/2
Laser
X
y
Reflectance
recorded

(b)

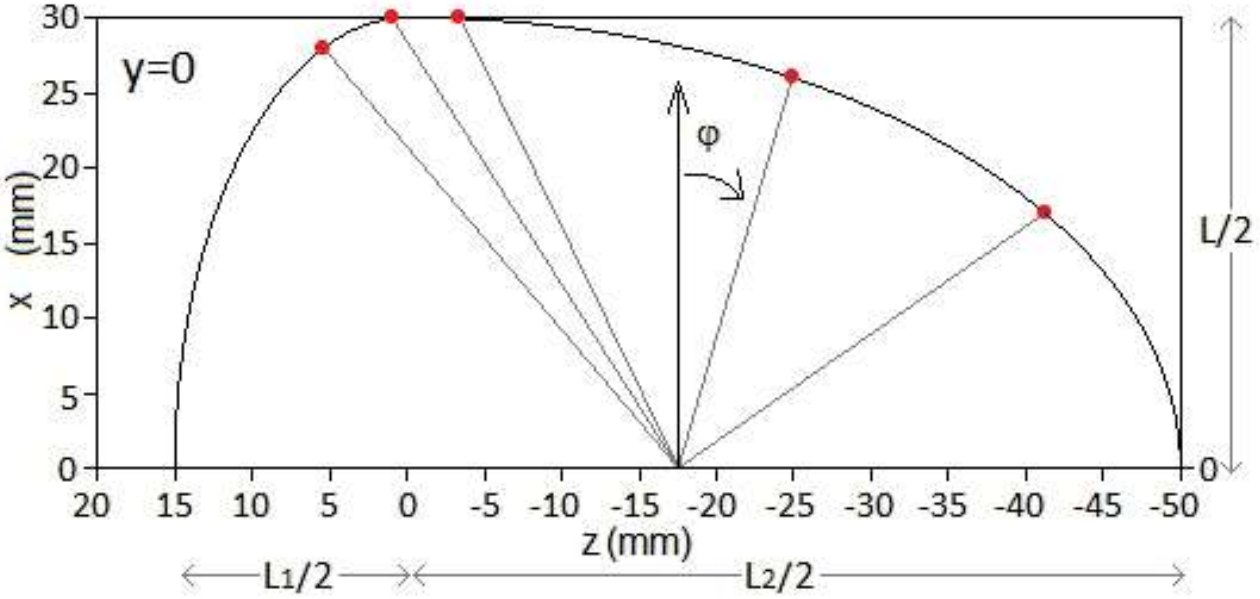
y=0
φ
x (mm)
z (mm)
L/2
L1/2
L2/2
30
25
20
15
10
5
0
20 15 10 5 0 -5 -10 -15 -20 -25 -30 -35 -40 -45 -50

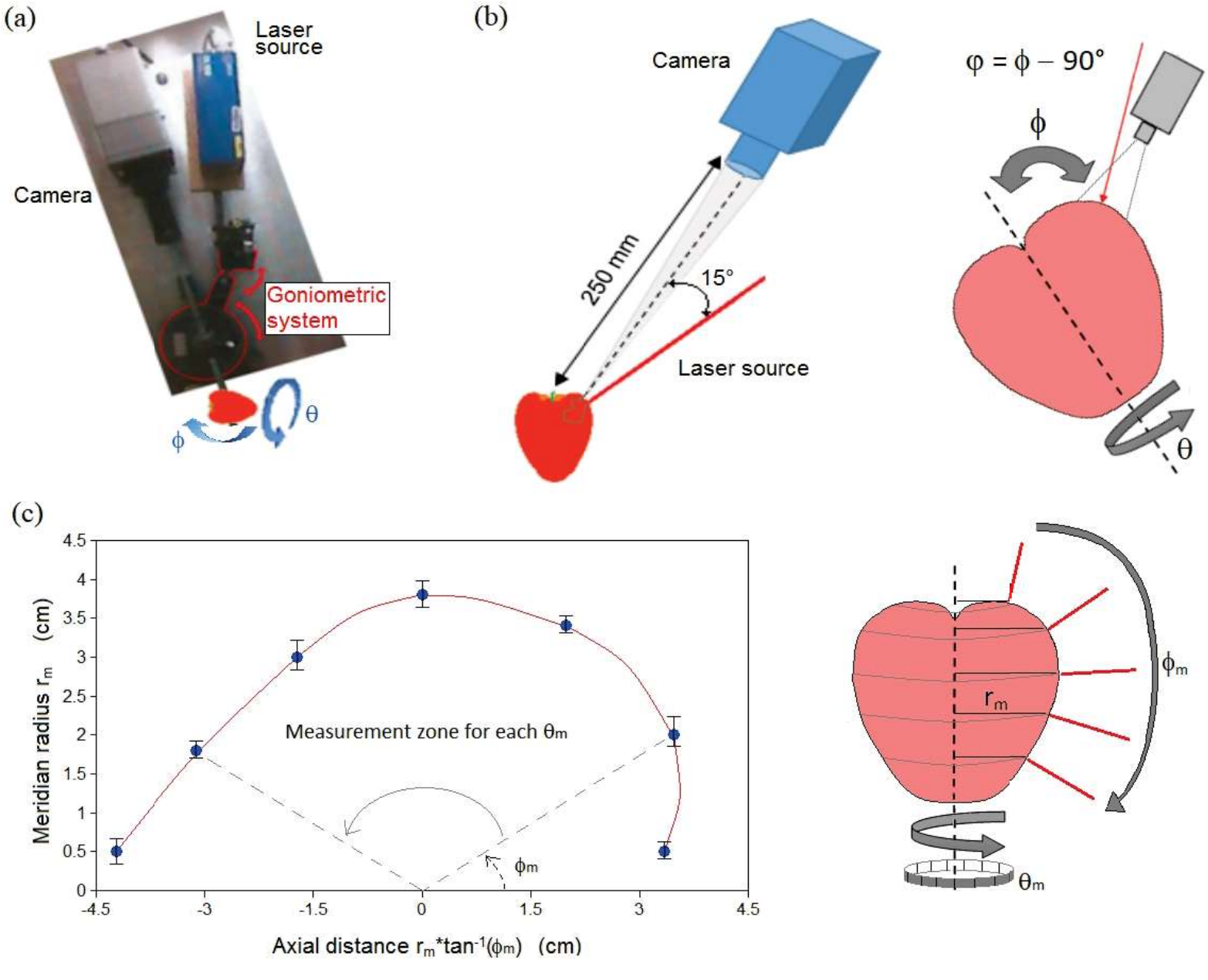
(a)
Laser source
Camera
Goniometric system
θ
ϕ
(b)
Camera
250 mm
15°
Laser source
φ = ϕ − 90°
ϕ
θ
(c)
Meridian radius r_m (cm)
Axial distance r_m*tan^{-1}(ϕm) (cm)
Measurement zone for each θm
ϕm
r_m
ϕm
θm

(a)

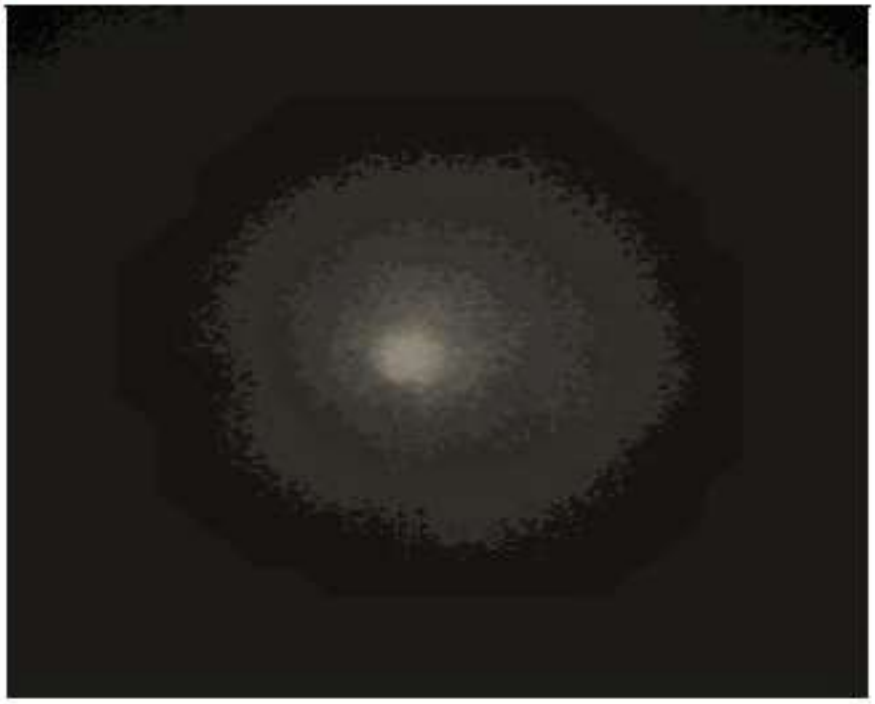

(b)

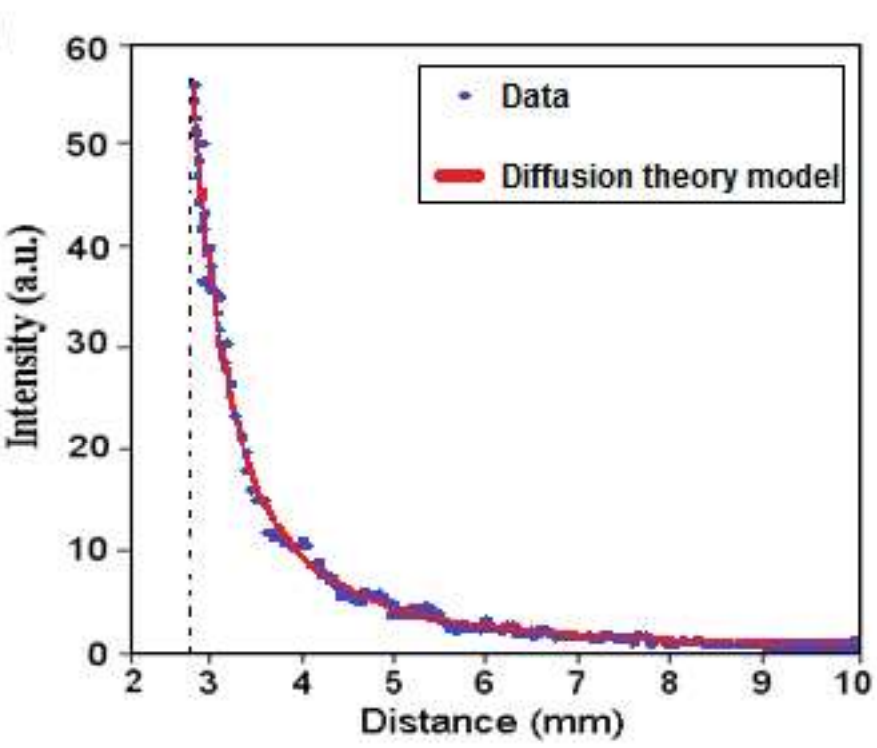
Data
Diffusion theory model
Intensity (a.u.)
Distance (mm)
0
10
20
30
40
50
60
2
3
4
5
6
7
8
9
10

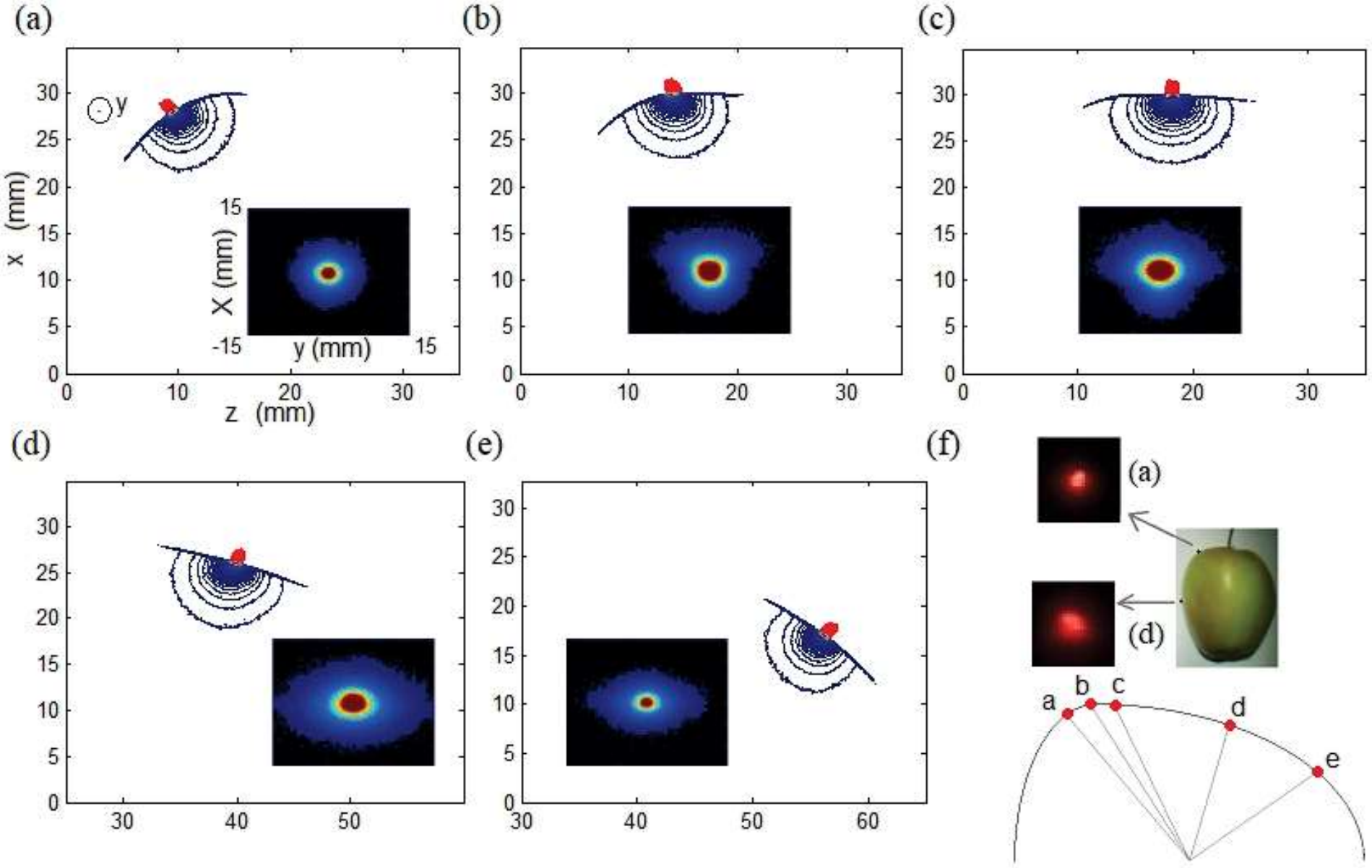
(a)
(b)
(c)
(d)
(e)
(f)
x (mm)
z (mm)
y
X (mm)
y (mm)
-15
15
(a)
(d)
a
b
c
d
e

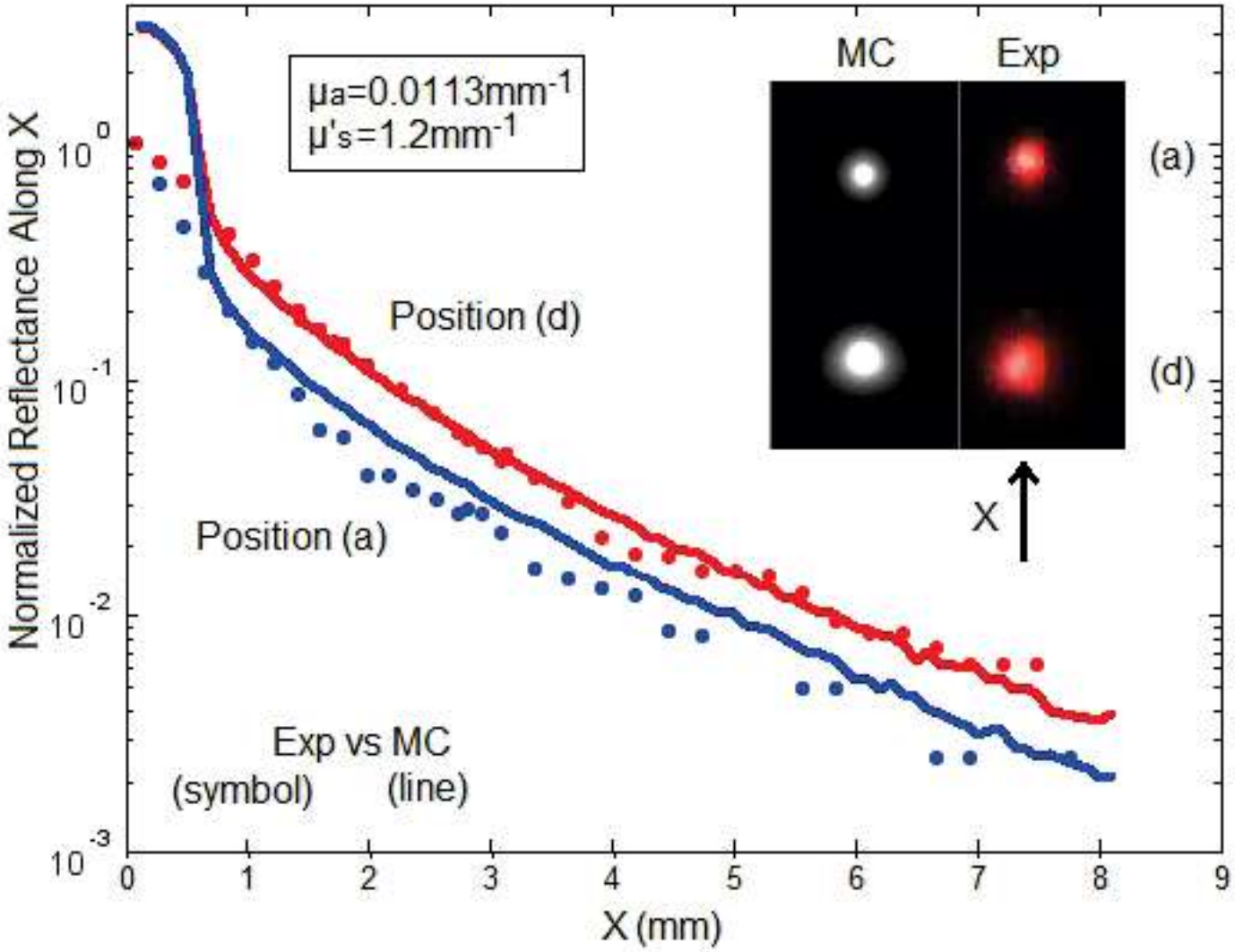
μa=0.0113mm-1
μ's=1.2mm-1
MC
Exp
(a)
(d)
X
Position (d)
Position (a)
Exp vs MC
(symbol) (line)
Normalized Reflectance Along X
X (mm)
10 0
10 -1
10 -2
10 -3
0
1
2
3
4
5
6
7
8
9

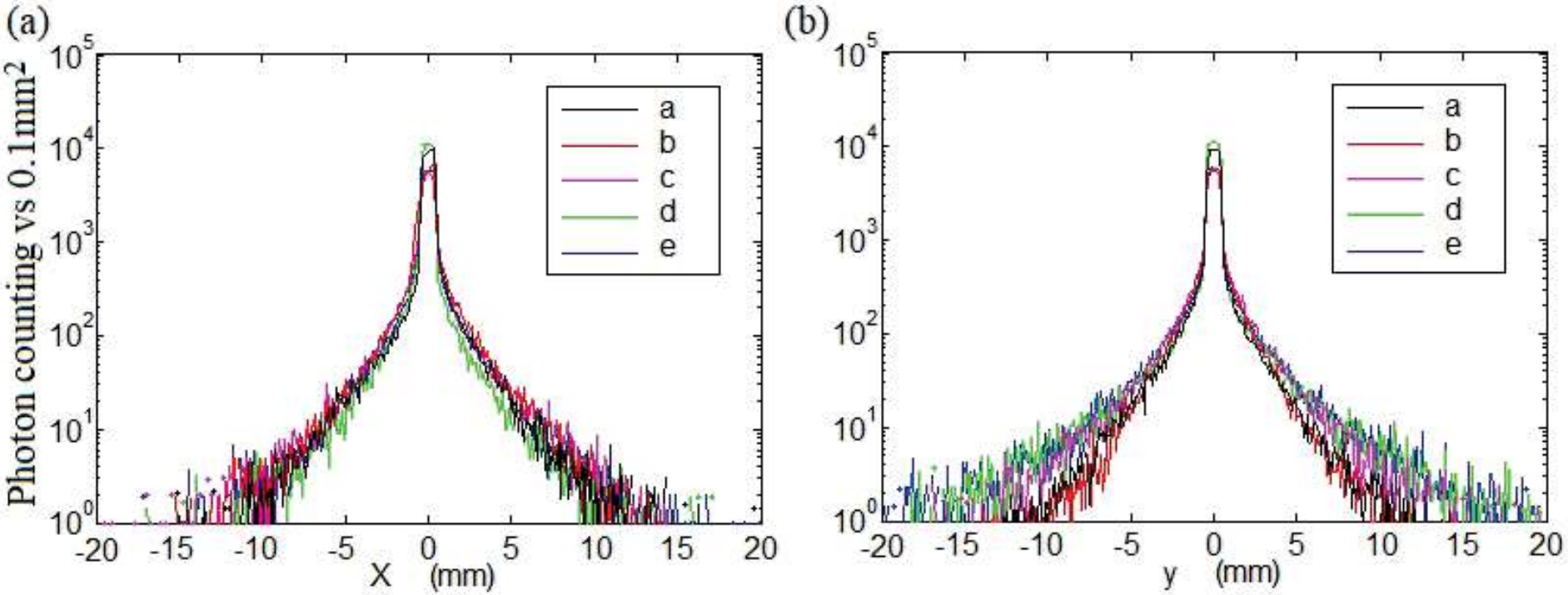
(a)
Photon counting vs 0.1mm²
10⁵
10⁴
10³
10²
10¹
10⁰
-20 -15 -10 -5 0 5 10 15 20
X (mm)
a
b
c
d
e
(b)
10⁵
10⁴
10³
10²
10¹
10⁰
-20 -15 -10 -5 0 5 10 15 20
y (mm)
a
b
c
d
e

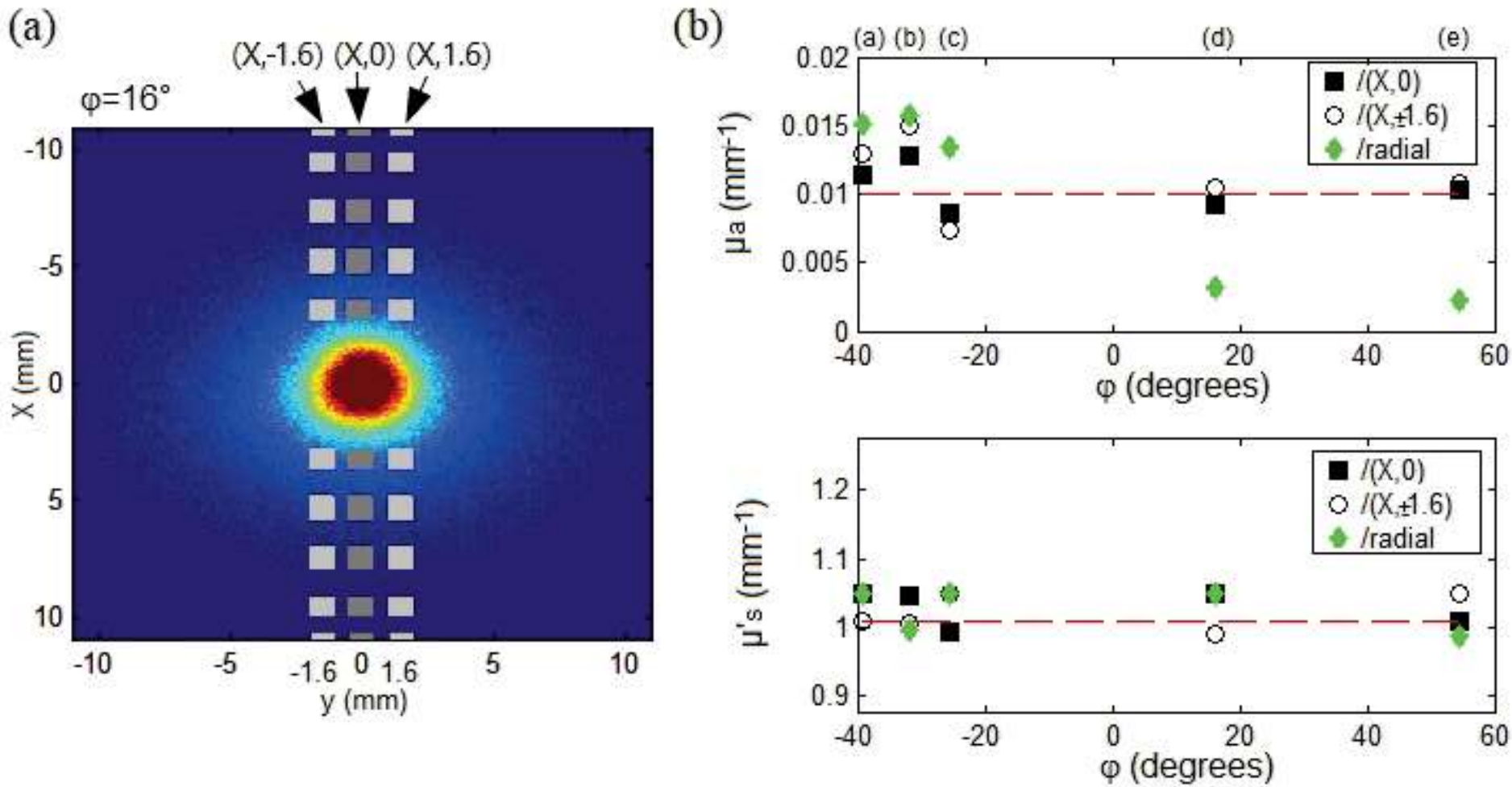
(a)
(X,-1.6) (X,0) (X,1.6)
φ=16°
X (mm)
y (mm)
(b)
(a) (b) (c)
(d)
(e)
μa (mm-1)
μ's (mm-1)
/(X,0)
/(X,±1.6)
/radial
φ (degrees)

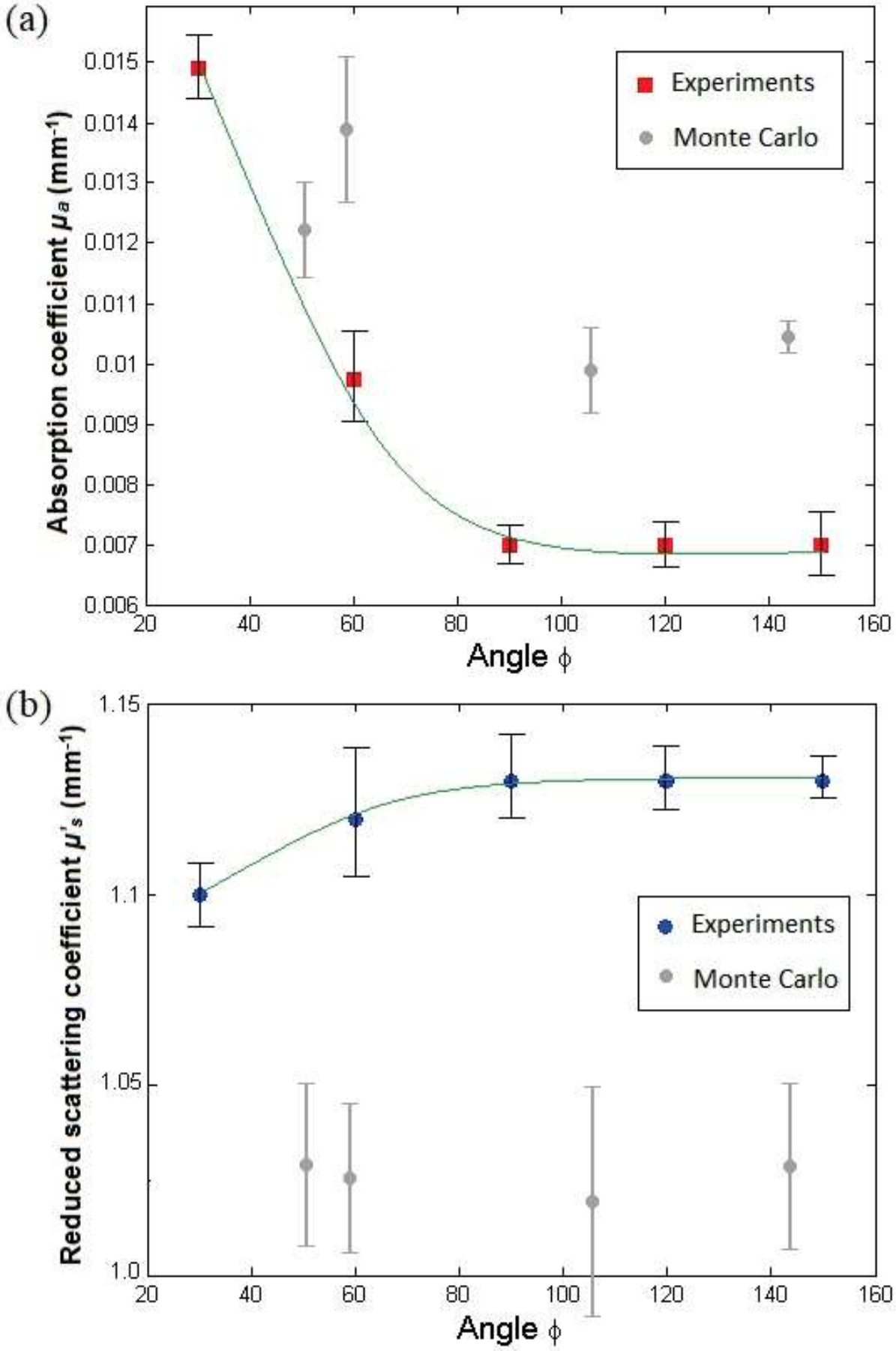
(a)
Absorption coefficient μ_a (mm^{-1})
0.015
0.014
0.013
0.012
0.011
0.01
0.009
0.008
0.007
0.006
20
40
60
80
100
120
140
160
Angle ϕ
Experiments
Monte Carlo
(b)
Reduced scattering coefficient μ'_s (mm^{-1})
1.15
1.1
1.05
1.0
20
40
60
80
100
120
140
160
Angle ϕ
Experiments
Monte Carlo

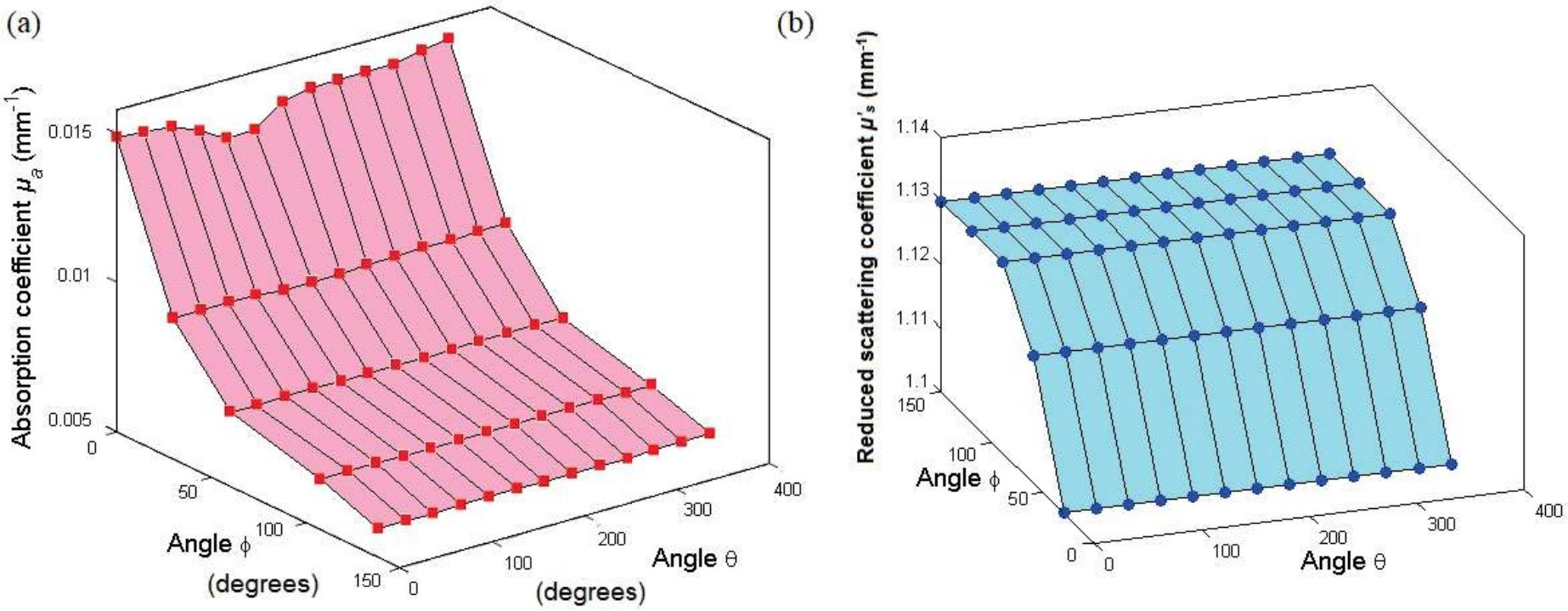
(a)
Absorption coefficient μ_a (mm^{-1})
0.015
0.01
0.005
0
50
100
150
Angle ϕ
(degrees)
0
100
200
300
400
Angle θ
(degrees)
(b)
Reduced scattering coefficient μ'_s (mm^{-1})
1.14
1.13
1.12
1.11
1.1
150
100
50
0
Angle ϕ
0
100
200
300
400
Angle θ

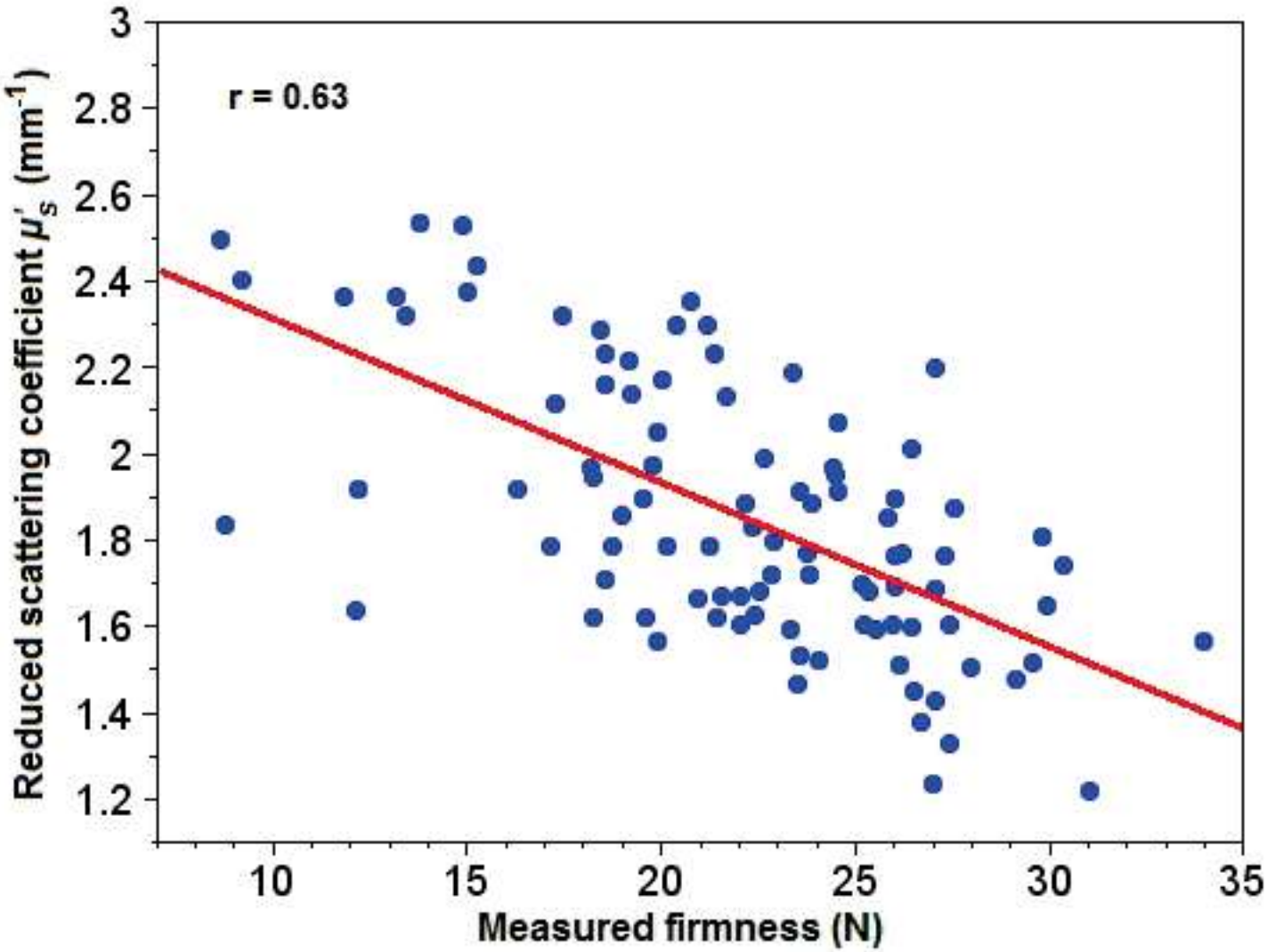
r = 0.63
Reduced scattering coefficient μ_s' (mm^{-1})
Measured firmness (N)
3
2.8
2.6
2.4
2.2
2
1.8
1.6
1.4
1.2
10
15
20
25
30
35